Cite this article
Francisca FM, Montoro MA and Mozejko CA
Detection of hydrocarbon spills by means of a coaxial impedance dielectric sensor.
Environmental Geotechnics,
https://doi.org/10.1680/jenge.22.00035

Research Article
Paper 2200035
Received 05/03/2022; Accepted 02/11/2022

Environmental Geotechnics

ice Publishing

Detection of hydrocarbon spills by means of a coaxial impedance dielectric sensor

1 **Franco M. Francisca** PhD, CEng
Professor, Department of Civil Constructions, Universidad Nacional de Córdoba, Cordoba, Argentina; Principal Researcher, Institute for Advanced Studies in Engineering and Technology, Universidad Nacional de Córdoba and Consejo Nacional de Investigaciones Científicas y Técnicas, Cordoba, Argentina (Orcid:0000-0002-6965-9036) (corresponding author: franco.francisca@unc.edu.ar)

2 **Marcos A. Montoro** PhD, MSc (CE), CEng
Adjunct Professor, Department of Civil Constructions, Universidad Nacional de Córdoba, Cordoba, Argentina; Adjunct Researcher, Institute for Advanced Studies in Engineering and Technology, Universidad Nacional de Córdoba and Consejo Nacional de Investigaciones Científicas y Técnicas, Cordoba, Argentina (Orcid:0000-0002-0533-3782)

3 **Clara A. Mozejko** MSc (CE), CEng
Adjunct Professor, Department of Civil Constructions, Universidad Nacional de Córdoba, Cordoba, Argentina; Institute for Advanced Studies in Engineering and Technology, Universidad Nacional de Córdoba and Consejo Nacional de Investigaciones Científicas y Técnicas, Cordoba, Argentina (Orcid:0000-0001-9909-979X)

Leakages from storage tanks or pipes frequently produce pollution of soils and groundwater reservoirs by hydrocarbons. Common practices for monitoring and characterising site contamination involve soil drilling, sampling and chemical analysis, complemented with geophysical surveys. This study evaluates the presence of paraffin oil inside soil pores by means of dielectric permittivity measurements, using a coaxial impedance device in laboratory-scale models. The real dielectric permittivity of unsaturated sand is measured before, during and after a contamination process. Monitoring small variations in real dielectric permittivity allows detection of the partial replacement of air ($\kappa' = 1$) by paraffin oil ($\kappa' \approx 2$) in soil pores. These variations in soil dielectric properties enable pollution levels to be assessed, knowing in advance the κ' of the soil at the initial stage and measuring the influence of oil and water content on κ'. The technique proposed can also be used for monitoring the lateral extension of a contaminant plume and can be successfully applied at the laboratory scale for oil leakage detection by periodically monitoring changes in the soil dielectric permittivity.

Keywords: geoenvironment/monitoring/pollution/porous-media characterisation/UN SDG 15: Life on land

Notation

c	fitting parameter in the dielectric permittivity mixture formula (dimensionless)
d_{10}	effective particle diameter (mm)
d_{50}	mean particle diameter (mm)
j	imaginary unit = $-1^{1/2}$
n	porosity (dimensionless)
S	degree of saturation (dimensionless)
w	soil moisture (dimensionless)
α	relative amount of sand contaminated with oil with respect to clean sand (dimensionless)
γ_d	dry unit weight (kN/m^3)
ε^*	complex dielectric permittivity (F/m)
ε_0	free space permittivity (8.85×10^{-12} F/m)
θ	volumetric liquid content (dimensionless)
θ_{oil}	relative volume of oil within the pores (dimensionless)
θ_w	relative volume of water within the pores (dimensionless)
κ^*	relative dielectric permittivity (dimensionless)
κ'	real component of the relative dielectric permittivity (dimensionless)
κ''	imaginary component of the relative dielectric permittivity (dimensionless)
κ^*_{eff}	relative permittivity of the heterogeneous phase mixture (dimensionless)
κ'_{so}	real permittivity of soil–paraffin oil at any volumetric content of liquid (dimensionless)
κ'_{sw}	real permittivity of soil–water at any volumetric content of liquid (dimensionless)

Introduction

Soils and groundwater are often contaminated by complex organic mixtures known as non-aqueous phase liquids (NAPLs). NAPLs can be classified in two different groups: denser-than-water NAPLs (DNAPLs) and lighter-than-water NAPLs (LNAPLs). After a spill or a leakage into the ground subsurface, NAPLs may flow downwards through the vadose zone until they reach the water table. In this way, part of the NAPL will remain trapped

inside soil pores, forming ganglia due to capillary forces (Francisca and Montoro, 2015; Halihan *et al*., 2017; Rinaldi and Francisca, 2006). If the leakage volume is important, the NAPL will pool and spread laterally when reaching the water table, in the case of LNAPLs, or will continue flowing downwards into the aquifer until it reaches a very low hydraulic conductivity layer over which it will pool, in the case of DNAPLs (Castelluccio *et al*., 2018; Newell *et al*., 1995). In all cases, the NAPL displacement inside the soil pores is governed by forces of gravity, capillarity and viscosity.

Accidental spills of hydrocarbons endanger environmental quality and are a major environmental concern nowadays (Gupta *et al*., 2020; Lim *et al*., 2016). Such contamination processes are likely to be found in urban and non-urban areas associated with leakages from pipelines or buried tanks at gas stations or during transportation by road or rail (Ramezanzadeh *et al*., 2022; Sharma and Reddy, 2004). This may lead to adverse impacts on ecosystems and potential risk to plant, animal and human health (Sharma *et al*., 2020), as well as changes in the physical, hydraulic and mechanical properties of soil (Fernandez and Quigley, 1985; Gnanapragasam *et al*., 1995; Khamehchiyan *et al*., 2007; Montoro and Francisca, 2010; Puri, 2000). Eventually, these modified properties may also affect in situ remediation processes, possible alternative uses of the contaminated soil and the performance of the existing foundation structures of neighbouring buildings and facilities (Abousina *et al*., 2015; Estrabagh *et al*., 2014; Kermani and Ebadi, 2012; Khamehchiyan *et al*., 2007).

These organic fluids have also very low solubility. However, a low concentration in water is considered dangerous for human health by many regulatory agencies around the world, and in consequence, hydrocarbon ganglia are considered a long-term contamination source and a severe environmental risk (Coulon *et al*., 2010; Farthing *et al*., 2012; Govindarajan *et al*., 2018; Le Meur *et al*., 2021; Sharma and Reddy 2004). Therefore, besides the importance of quantifying the affected area and conducting remediation actions (Lee *et al*., 2019), adequate delineation of the extent and thickness of contaminated sediments is critical to understanding risk at contaminated sites (Alimohammadi *et al*., 2020; Davidson *et al*., 2021; Davis *et al*., 2018).

There are two main traditional detection and monitoring strategies for site characterisation. The first group involves installation of monitoring wells (Cecconi *et al*., 2022), combined with soil and groundwater drilling and core sampling, complemented with laboratory tests (Comegna *et al*., 2016; Newell *et al*., 1995; Yoon *et al*., 2013). The main limitations of these techniques based on sampling and geochemical analysis are related to expenses associated with the drilling and sampling processes (Halihan *et al*., 2017), combined with the fact that hydrocarbons do not displace uniformly inside soil pores, providing limited spatial and temporal resolution. In this way, oil inside soil pores cannot be rapidly detected by using only traditional methods, and consequently, high degrees of contamination cannot be prevented. The second group involves using indirect subsurface measurements with geophysical techniques (Power *et al*., 2015). These non-invasive methods have been studied in the recent years and offer an attractive alternative for contaminated site characterisation (Comegna *et al*., 2013; Kessouri *et al*., 2022; Redman *et al*., 1991).

Different geophysical methods have been proposed as economical and practical tools for monitoring contamination processes and for characterising contaminated sites before and after remediation actions (Francisca and Montoro, 2012; Power *et al*., 2015). Complex organic compounds are highly resistive fluids. When replacing water in a porous media they usually provide a strong electrical contrast (Halihan *et al*., 2017; Kafarski *et al*., 2019; Singha *et al*., 2015). This resistive contrast enables easy and fast contamination site characterisation. Dielectric techniques are widely accepted for this purpose and are based on the principle of electromagnetic wave propagation. These methods can operate under a low frequency (LF) or a high frequency (HF).

Electrical resistivity tomography (ERT) and induced polarisation (IP) are the most widely used LF techniques (Revil *et al*., 2012). ERT is a very popular geophysical imaging technique due to the significant contrast in soil resistivity produced by changes in moisture content and/or the presence of contaminant fluids in soil pores (Johansson *et al*., 2015; Power *et al*., 2015; Tsai *et al*., 2020). ERT has been applied for contaminant mapping and monitoring because it is possible to assess spatial and temporal changes due to the presence of pollutants (Tsai *et al*., 2020). IP tomography is widely recognised as a valuable tool for determining the impact of NAPL contamination in the subsurface (Deceuster and Kaufmann, 2012). However, both methods (ERT and IP) present some practical limitations in their field applications. Among the most important issues are the interpretation of measured data, which is importantly affected not only by the presence of contaminants from unknown sources but also by the complexity of local geological and hydrogeological conditions (Power *et al*., 2014), which may produce stronger resistivity variations than those associated with the presence of NAPLs (Deng *et al*., 2017). Also, both the electrical and the electromagnetic responses of contaminant fluids are influenced by their stage of degradation (Cassidy, 2007; Tsai *et al*., 2020). The final limitations of ERT and IP tomography are the reliability of the signal interpretation and the complex inversion algorithms required for their numerical processing (Cardarelli and Di Filippo, 2009; Koohbor *et al*., 2022; Power *et al*., 2014).

Among HF methods, the most accepted techniques include GPR, time domain reflectometry (TDR) and coaxial impedance dielectric reflectometry (CIDR), which are based on the indirect detection of soil resistivity and conductivity parameters (Benson and Bosscher, 1999; Cassidy, 2007; Cataldo *et al*., 2014; Comegna *et al*., 2019; Francisca and Rinaldi, 2003; Francisca *et al*., 2012; Knight, 2001). These techniques were successfully

used to measure the moisture content of soils (Mu *et al*., 2020; Suchorab *et al*., 2020), changes in groundwater levels (Cao *et al*., 2020; Nemarich, 2001), tree stem moisture (He *et al*., 2021), pollutant migration (Cassidy, 2007; Glaser *et al*., 2012; Lau *et al*., 2021) and the moisture content of waste in landfills (Dawrea *etal*., 2021); to detect buried objects (Xie *et al*., 2020); and to monitor pipe leakage (Cataldo *et al*., 2014; Liu *et al*., 2013) and oil tank leakage (Lee *et al*., 2019). The main limitation of these techniques is linked to the fact that organic liquid detection in soils is restricted to high contaminant concentration levels if the initial soil condition is not known in advance (Francisca and Rinaldi, 2001).

Even though several contaminant-monitoring systems exist nowadays, a significant deficit subsists regarding early spill detection systems. There is also a lack of research regarding this problem. Traditionally, contaminant site characterisation combining traditional and geophysical methods is performed after notification of an NAPL spill occurrence. However, early NAPL spill detection at storage plants or transport facilities due to prior installation and system preparation is uncommon. The set-up for an early detection system requires a permanently installed sensor at a specific site, which must be capable of capturing small variations in soil dielectric properties. For this, CIDR probes prove to be a versatile, economic, reliable and easy-to-operate solution. Furthermore, data acquisition is manageable, as time-measuring intervals can be as short as minutes, favouring continuous monitoring. Besides these advantages, the results obtained are also easy to analyse when compared with those by TDR probes. On the other hand, ground-penetrating radar (GPR) systems, for example, cannot be permanently installed, and therefore, frequent surveys may be planned and spills may be detected only when analysing differences in the results between consecutive surveys.

Permanent in situ installed sensors allow changes in dielectric properties to be detected, which may be associated with contaminant presence. The main objective of this study is to evaluate the ability of CIDR to determine the dielectric permittivity of contaminated and uncontaminated soils. The main goal is to determine if the proposed HF method can be used as a reliable tool for early detection of contaminants, focusing on the ability to detect quickly changes in the real relative dielectric permittivity component of the soil when an immiscible organic liquid comes into contact with the granular soil matrix, resulting in a low-cost system for monitoring hydrocarbon spills and displacements in field applications, such as the early detection of soil contamination.

Detection principle

Geophysical methods are based on either electromagnetic wave propagation or reflection when soil changes its electromagnetic impedance, which is mainly controlled by the present phases of the heterogeneous phase mixture that form soils: mineral particles, water, ionic solutions, air, oil and their individual dielectric properties (Francisca and Rinaldi, 2003).

The dielectric permittivity of soils is a complex parameter that can be defined as follows:

$$\kappa^* = \frac{\varepsilon^*}{\varepsilon_0} = \kappa' - j\kappa'' \quad (1)$$

where ε^* is the complex dielectric permittivity, ε_0 is the free space permittivity (8.85×10^{-12} F/m), κ^* is the complex relative permittivity, j is the imaginary unit and κ' and κ'' are the real and imaginary components of the complex relative permittivity, respectively. The real component κ' (or dielectric constant) is a dimensionless parameter that captures the ability of a molecule to be aligned in the direction of an external electric field, while the imaginary component κ'', also dimensionless, represents the electrical conductivity and conduction losses due to the varying electromagnetic field.

The dielectric permittivity of soils depends on the different present phases, their temperature, their electromagnetic properties, the measurement frequency, the volumetric content of each phase and the possible interaction between these phases (Atekwana *et al*., 2006; Deceuster and Kaufmann, 2012; Rinaldi and Francisca, 1999). The dielectric permittivities in the megahertz frequency range of the different phases present in a contaminated soil at a temperature of 20°C are as follows: pure water, $\kappa' = 78.5$ (Kaatze, 1993); oil, $\kappa' \approx 2$ (Francisca and Rinaldi, 2003); mineral particles, $\kappa' \sim 5.5$; and air, $\kappa' = 1$ (Santamarina and Fam, 1997; Seyfried and Murdock, 2004; Thevanayagam, 1995). Pure water has a relatively constant dielectric permittivity in the megahertz frequency range, showing neither relaxation nor dispersion (Francisca and Rinaldi, 2003; Kaatze, 1993). In the same frequency range, hydrocarbons have a nearly constant κ' value that ranges from 2.01 to 2.46 for different types of oils (Francisca and Rinaldi, 2003). The dielectric permittivity of common minerals and rocks ranges from 4 to 9 (Parkhomenko, 1967), with $\kappa' \sim 5.5$ being a typical value for silica. Thus, the higher the amount of water, the higher the dielectric permittivity of the soil.

There are two different strategies for determining the relative volumetric content of each phase in a contaminated soil sample from measurement of the dielectric constant: using empirical conversion equations or using dielectric mixing models. Using the first approach means that empirical conversion equations need to be calibrated for different type of soils and liquids, while using dielectric mixing models requires knowing in advance the dielectric permittivity of the pure materials present in the mixture (Černý, 2009). The first strategy is usually applied to quantify the soil volumetric water content, with Topp's equation (Topp *et al*., 1980) being the most popular equation for this purpose. Regarding the second approach, the dielectric permittivity of

phase mixtures may be predicted from effective medium models and the electrical response of equivalent circuits (Macdonald, 1987; Mohamed and Paleologos, 2018; Rinaldi and Francisca 1999).

The most general equation for mixing models is Lichtenecker's formula:

$$2. \quad \kappa_{\text{eff}}^{*\,c} = \sum_i \theta_i \kappa_i^{*c}$$

where κ_{eff}^{*} is the dielectric permittivity of the phase mixture, c is a constant that varies between −1 and 1 and κ_i^{*} and θ_i are the permittivity and the relative volume of the 'i' phase, respectively. A constant c is frequently adopted as a fitting parameter, but when adopting extreme values, Equation 2 gives the response of equivalent electrical circuits in parallel and series, which are known as Wiener's upper and lower bound limits, respectively. When c = 1/3, the equation is known as Looyenga's model, and if c is equal to 1/2, the equation is known as the complex refractive index (CRIM) model.

Contaminated soils can be considered phase mixtures (Francisca and Rinaldi, 2003). In this case, the main objective when performing dielectric measurements is either contaminant detection or determination of the relative amount of the contaminant present in the soil pores. The use of effective medium models or mixing models requires the extension of these models from two- (and three-) to four-phase mixtures to be able to predict the dielectric responses of contaminated soils due to the presence of solid particles, air, water and NAPL. In this way, Francisca and Montoro (2012) developed a quantitative procedure by which the real dielectric permittivity of four-phase mixtures can be obtained from calibration curves when the dielectric responses of soil–water (κ'_{sw}) and soil–organic mixtures (κ'_{so}) are previously known, as follows:

$$3. \quad \kappa_{\text{eff}}^{\prime c} = \alpha \kappa_{\text{so}}^{\prime c} + (1 - \alpha)\kappa_{\text{sw}}^{\prime c}$$

where κ'_{eff}, κ'_{sw} and κ'_{so} are the real dielectric permittivities of effective media, soil–water and soil–oil at the same liquid volumetric content; c is a fitting parameter included to maintain similarity with Equation 2; and α is the relative amount of soil contaminated with oil mixed with clean sand. Thus, the possible values of α range between 0 and 1. Assuming constant porosity, the parameter α is found by (Francisca and Montoro, 2012)

$$4. \quad \alpha = \frac{\theta_{\text{oil}}}{\theta_{\text{w}} + \theta_{\text{oil}}}$$

where θ_{oil} and θ_{w} are the relative volumes of oil and water in the pores, respectively. Note that Equation 3 becomes equal to Equation 2 when κ'_{sw} and κ'_{so} are expressed as two-phase mixtures (particles and water and particles and oil, respectively).

Materials and methods

Soils and fluids

The soil employed for all the tests performed corresponds to a fine sand obtained from the Anisacate River, located in the province of Cordoba, Argentina. A qualitative optical diffraction test shows this sand as mainly composed of pure minerals such as silica, feldspar, muscovite and rock fragments mostly from granite. The sand has a mean particle diameter of d_{50} = 0.3 mm and an effective particle diameter of d_{10} = 0.1 mm. Its grain size distribution presents a coefficient of uniformity of 3.3 and a coefficient of curvature of 1.2. Thus, the sand classifies as SP according to the Unified Soil Classification System (ASTM D 2487 (ASTM, 2017)). Clean sands were used in the laboratory tests to avoid deviations from difficulty in the interpretation procedure due to the effect of electrical double-layer interactions that are expected to occur in clay mineral particles (Colombano *et al*., 2021; Dirksen and Gasberg, 1993).

Tap water and paraffin oil were used as mixing liquids for all tests. The paraffin oil used as an immiscible organic contaminant had a relative density of 0.846 and a dynamic viscosity of 1.5 × 10^{-2} N s/m^2. The real dielectric permittivity of the paraffin oil was $\kappa'_{\text{po}} = 2.01$, which is approximately 40 times smaller than the real component of the dielectric permittivity of water, $\kappa'_{\text{w}} = 78.5$. The difference in real permittivity allows changes in the dielectric permittivity of contaminated and uncontaminated soil to be identified (Francisca and Rinaldi, 2003; Montoro and Francisca, 2008).

Dielectric permittivity probe

Dielectric permittivity measurements were performed with the HydraProbe soil sensor, using CIDR, manufactured by Stevens Water Monitoring Systems Inc. The probe is composed of four metal tines, 6 cm long. Three of these tines are disposed in an equilateral triangle, while the fourth is placed at the centre. The three outer tines define a cylindrical measurement volume of 2.5 cm diameter and 6 cm height (Figure 1).

A 50 MHz electromagnetic wave is generated and transmitted to the sample by the tines. The dielectric permittivity is determined by the changes in amplitude between the transmitted and reflected waves, so the probe enables the real and imaginary components of the dielectric permittivity to be determined. Seyfried and Murdock (2004) performed HydraProbe calibrations to determine soil water content, conducting measurements on different types of soils with different water contents and also with water with different salt concentrations. They found that measurements are accurate and precise when $\kappa'' <$ 50 and $\tan\delta < 1.45$. The sensor has a real dielectric permittivity range between 1 and 80 with an accuracy of ±0.5%. The bulk electrical conductivity measurement range is between 0 and 1.5 S/m, with an accuracy of ±0.02 S/m, according to the supplier's information.

Figure 1. Experimental set-up for dielectric permittivity determination of sand samples with different amounts of fluids using the HydraProbe sensor

However, this study analyses only the real component of dielectric permittivity. The influence of the volumetric content of oil on the imaginary permittivity of soils can be obtained from the studies by Francisca (2001) and Rinaldi and Francisca (2006).

The dielectric probe measures the κ' and κ'' of the material surrounded by the three external tines that defines the cylindrical measurement volume (Figure 1). According to Seyfried *et al.* (2005) the measurements provide the arithmetic average of the dielectric permittivities of the materials located within this zone (e.g. minerals particles, air, water, oil). Given that measurement frequency is 50 MHz, the HydraProbe wavelength is near 6 m. This represents more than four times the full length of the sensing volume (6 cm), and therefore it is significantly greater than any spatial heterogeneity that could be generated within the cylindrical measurement volume. In this case, the probe provides average values with negligible scattering effects (dielectric permittivity remains constant in the megahertz frequency range (Francisca and Rinaldi, 2003)), so the material under test can be considered an effective medium (Bore *et al.*, 2021). This spatial sensitivity analysis and the linear average of dielectric permittivity within the sensing volume were experimentally confirmed by Francisca and Montoro (2012). Therefore, small anomalies cannot be detected given that they produce differences in the effective dielectric permittivity lower than the accuracy of the probe (±0.5%).

The probe is constructed in such a way that it can resist contact with hazardous and corrosive substances for long periods of time and can be placed under the phreatic level.

Experimental procedure

Four different experiments were performed in this research. The first group of experiments consisted of determining the variation of the real component of dielectric permittivity with changes in either the water and/or paraffin oil content in the soil sample. Different mixtures of dry sand with a known content of either water and/or paraffin oil were placed in a glass beaker, 10 cm tall and 5 cm diameter (Figure 1). The relative volume of the liquid phase to the volume of the mixture varied from 0 to nearly 38% with the following paraffin oil (PO)–water (w) ratios: 0% PO–100% w, 50% PO–50% w and 100% PO–0% w, which correspond to $\alpha = 0$, 0.5 and 1.0, respectively (Equation 3). The highest volumetric contents of liquids were close to sample porosity to ensure a degree of saturation close to 1. The sensing probe was carefully introduced into the sand to measure the dielectric permittivity of the sand–water, sand–paraffin oil and sand–water–paraffin oil mixtures.

The second group of experiments consisted of determining the size and shape of a controlled paraffin oil spill. A stainless-steel recipient, 59 cm long, 39 cm wide and 10 cm tall, was used to perform this experiment. The schematic laboratory set-up is presented in Figure 2(a). For this experiment, twin samples were prepared by filling the cell with wet sand ($w = 10\%$ by weight) with a mean porosity of $n = 0.38$ and dry unit weight $\gamma_d = 16$ kN/m^3 in both recipients. One sample was kept as the reference situation, while 3200 cm^3 of paraffin oil was discharged at the centre of the cell through a filtrating surface of 23 cm per 16 cm in the second sample (see Figures 2(a)–2(c)). Then, both sample surfaces were divided into 143 squares of 4.5 cm per 3.5 cm, and the probe was introduced at the centre of each square, verifying that the measurements of dielectric permittivity were made at the same locations in each sample. The dielectric permittivity measurements in the first sample gave a reference value to show the expected influence of any spatial variability effect of soil properties on dielectric permittivity due to small porosity changes during the preparation procedure. Dielectric permittivity measurement in the second sample enabled comparison between this sample and the first sample to identify the extent of the paraffin oil spill.

The third type of experiment consisted of preparing a specimen with a known contaminated region. The same recipient was used as in the previous experiment, but in this case, the specimens were intentionally prepared with heterogeneous distributions of sand–water and sand–paraffin oil. The heterogeneous sample was prepared with a rhombohedral region at the centre, which was filled with contaminated sand (paraffin oil content $w = 25\%$ by weight), and the surrounding space was filled with clean sand

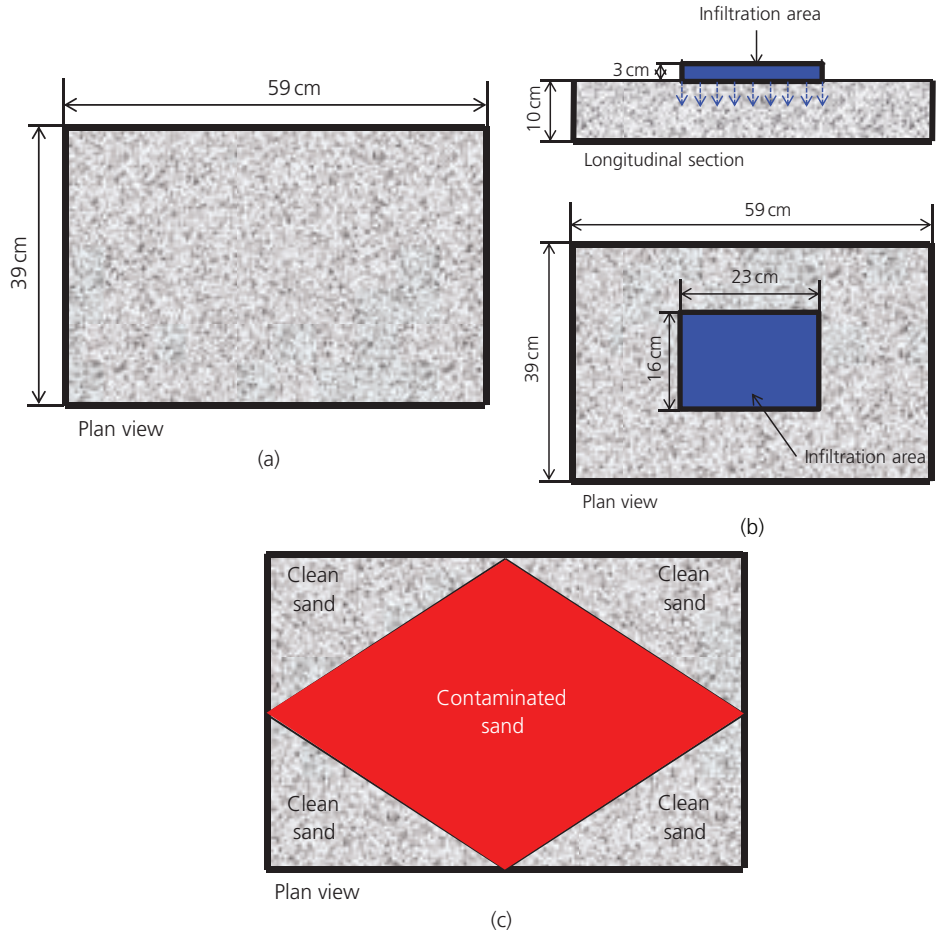

Figure 2. Experimental set-ups for tests performed with fine sand: (a) uniform fine sand initially moistened with water with a central infiltration area for paraffin oil, plan view; (b) longitudinal section of the uniform fine sand sample; (c) geometrical arrangement of the fine sand sample composed by clean water-moistened sand and a central rhombohedral region of paraffin oil-contaminated sand

(water content $w = 25\%$ by weight) (Figure 2(b)). Both clean and contaminated sand had a saturation degree of $S \approx 1$; the mean dry unit weight of the sample was $\gamma_d = 16\ \text{kN/m}^3$, and the volumetric content of the liquid was $\theta \approx n = 0.38$. The surface of the sample was also divided into 143 squares of 4.5 cm per 3.5 cm and the dielectric probe was introduced at the centre of each square in order to measure the dielectric permittivity. In this experiment, the clean and contaminated areas were known in advance, and therefore, the dielectric measurements were performed to evaluate the detectability of areas contaminated with paraffin oil.

The last group of experiments consisted of the detection of a paraffin oil spill in unsaturated sand. Sands with a moisture content of $w = 5\%$ by weight was placed in a cell 35 cm long, 25 cm wide and 15 cm tall. The wet sand was poured and compacted in the container, and when it reached 6.8 cm from the bottom, the dielectric probe was disposed in a horizontal direction towards the centre of the cell, after which the container was completely filled (Figure 3). A piezometer was connected to a

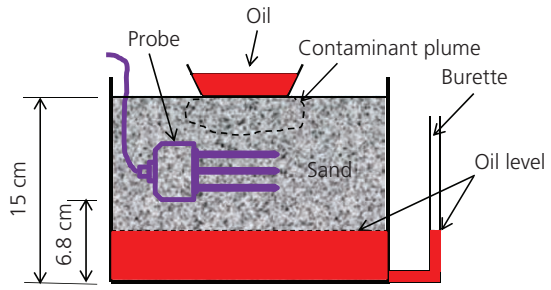

Figure 3. Experimental set-up of the paraffin oil continuous infiltration test in a uniform fine sand sample with the buried probe

port placed at the bottom of the container to monitor the position of the liquid level inside the sample. After filling the cell with wet sand, paraffin oil was gradually spilled at a constant rate while the dielectric permittivity was measured every 100 cm^3 of paraffin oil introduced in the sample (Figure 3(b)).

Results

Figure 4 shows the influence of the volumetric content of liquid on the real dielectric permittivity on sand for the first group of experiments, when the mixing fluids were water, paraffin oil and water–paraffin oil (50%–50%). As can be seen, the real dielectric permittivity of the sand–water mixtures is higher than that of the sand–paraffin oil mixtures, due to the higher κ' of water in comparison with that of paraffin oil. Although in both cases κ' rises with the volumetric content of liquid, in the presence of water, the increase in κ' becomes significant as water adopts values of $\kappa' \approx 78.5$, significantly higher than that of air with $\kappa' = 1$. Thus, the replacement of air by water inside the pores justifies the increase in κ' in the sand–water mixtures observed at higher fluid volumetric contents. A slight increase in κ' with the volumetric content may also be detected when working with sand–paraffin oil mixtures. This is attributed to the small difference between the κ' of paraffin oil ($\kappa' = 2.01$) and that of air ($\kappa' = 1$). The real dielectric permittivity of sand–paraffin oil–water (50% PO–50% w) shows intermediate values of κ' in comparison with those of clean sand–water mixtures (0% PO–100% w) and sand–paraffin oil mixtures (100% PO–0% w).

The real dielectric permittivities measured may be compared with the predicted values using dielectric mixing models. Effective medium models have the advantages of being of practical application and implementation, as they require knowledge only of the component permittivities of the materials and their fractional volume content. There are many studies previously published using effective medium models for determining NAPL contaminant content in soils and porous materials. Glaser *et al.* (2012) determined that parallel, serial, CRIM and Looyenga's models provided similar dielectric permittivity values when estimating that corresponding to Ottawa sand, ethanol and water mixtures. Moreover, recent results indicate that Looyenga's model

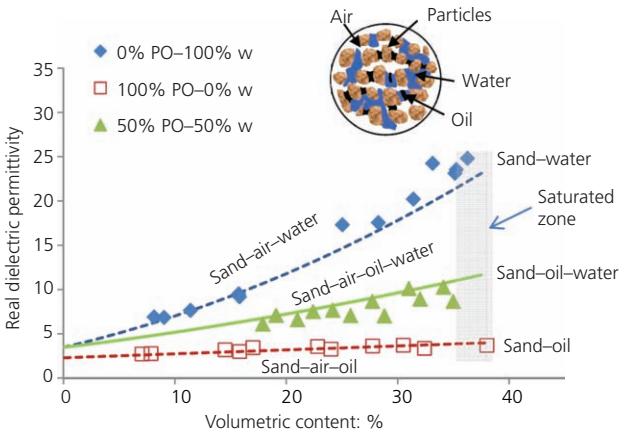

Figure 4. Real dielectric permittivity change for fine sand samples moistened with either water, paraffin oil or both fluids at different fluid volumetric contents. Lines represent results of the CRIM model (first group of experiments)

provides the best agreement with ethanol concentrations when modified to include a factor that takes into account a geometric term for the granular media (Glaser *et al.*, 2022). However, the CRIM model is one of the most widely used for hydrological applications and contaminant identification-related problems, as it is simple to apply and robust and gives accurate results for dielectric permittivities measured by HF methods (Cassidy, 2007; Colombano *et al.*, 2020). Persson and Berndtsson (2002) reported errors up to 5% for NAPL saturation of paraffin oil in sands. Besides, there are many sources that strengthen the use of CRIM models based on the accuracy of their results for different situations (Colombano *et al.*, 2020; Dirksen and Gasberg, 1993; Endres and Knight, 1992).

The real dielectric permittivity results obtained were fitted with Lichtenecker's model (Equation 2) using exponent $c = -1$, 1/3, 1/2 and 1. The best fit was obtained for exponent $c = 1/2$, showing that the CRIM model is the one that best fits the authors' experimental results, with a root mean square error (RMSE) of 1.59 in comparison with 6.76 for $c = -1$, 2.3 for $c = 1/3$ and 6.46 for $c = 1$. Figure 4 also shows a comparison between measured and expected real dielectric permittivities according to the CRIM model for sand–water and sand–paraffin oil (dashed line). For this test model, the parameters were porosity $n = 0.38$ and real dielectric permittivities of air $\kappa' = 1$; of water, $\kappa' = 78.5$; and of particles. $\kappa' = 5.5$. The liquid or saturation degree was considered variable, considering that the volumetric content of liquid, θ, depends on saturation, S, and porosity, n ($\theta = Sn$). The experimental results and the corresponding model responses provided the required calibration curves for the real dielectric permittivity of soil–water (κ'_{sw}) and soil–organic mixtures (κ'_{so}). From these values, the real dielectric permittivity of the 50% PO–50% w was computed from Equation 3 with $\alpha = 0.5$ and $c = 0.5$, as in the CRIM model (solid line in Figure 4). The real dielectric permittivities obtained properly represent the experimental data, showing the accuracy of the procedure to predict the dielectric behaviour of the contaminated sand. A similar analysis was performed for different relative volumes of paraffin oil with respect to water (different α in Equation 3). In all cases, the expected values fall between the upper and lower boundaries shown in Figure 4, which correspond to mixtures of soil–water–air and soil–paraffin oil–air, respectively.

Real dielectric permittivities lower than those corresponding to clean specimens (κ'_{sw}) indicate the presence of a contaminant. However, this is true only for a given volumetric content of liquid, considering that different air content and porosity values can also be responsible for dielectric changes, hiding the effect of contamination on κ'. Figure 5 presents a comparison between the experimental results reported in Figure 4 for κ' and κ' predicted with Francisca and Montoro`s model (Equation 3). The experimental results were obtained from measurements performed on sand–fluid mixtures, considering sand–water mixtures, sand–paraffin oil mixtures, both types of mixtures at different volumetric fluid content and mixtures of sand with both fluids

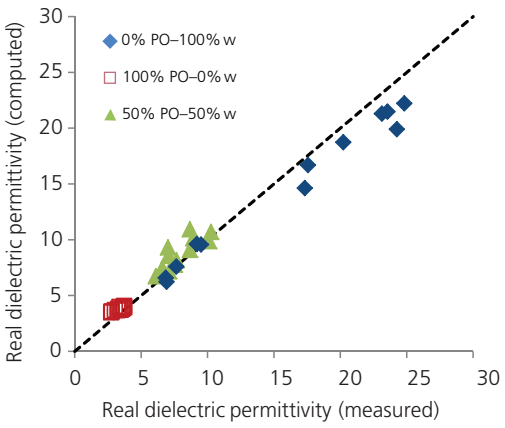

Figure 5. Comparison between real dielectric permittivities measured and predicted using the CRIM model and the Francisca and Montoro (2012) model for fine sand samples with different contents of water, paraffin oil or water–paraffin oil simultaneously (first group of experiments). PO, paraffin oil; w, water

simultaneously in the same volume proportion of each fluid. Symbols represent experimental results, and the dashed line represents the perfect fit line for Equation 3. Figure 6 shows the obtained absolute error and also indicates the RMSE as a measurement between the predicted and measured values.

The real dielectric permittivity of clean wet sand may have exactly the same value as that obtained for the same sand contaminated with paraffin oil, as shown in Figure 5. This may be explained by the relative contribution of the volumetric content and dielectric permittivity of the different phase mixtures, as previously reported in the literature. Therefore, the detection of oil in soils by means of dielectric permittivity is a difficult task (Cassidy, 2007; Flores Orozco *et al.*, 2012; Revil *et al.*, 2012; Tsai *et al.*, 2020).

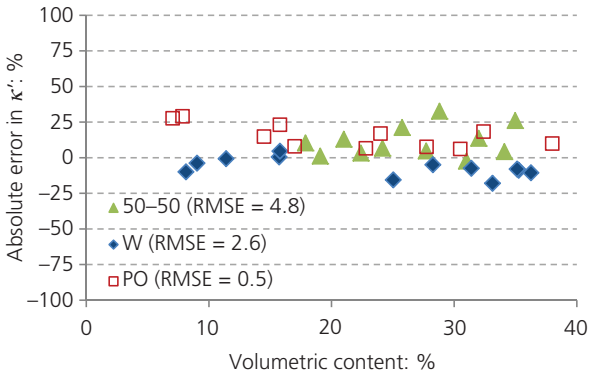

Figure 6. Absolute error and RMSE for the prediction of real dielectric permittivities using the CRIM model and the Francisca and Montoro (2012) model (first group of experiments). PO, paraffin oil; w, water

Figure 7 shows the results obtained for the second group of experiments. Figure 7(a) shows the dielectric permittivity map for a uniform fine sand sample compacted in the cell with an initial water moisture content equal to w = 10%. The maximum and minimum values of κ' are 11.64 and 9.01, respectively. Deviations of κ' within this range may be associated with local variations of either porosity or saturation, as expected according to Equation 3. In a twin sample, 3200 cm^3 of paraffin oil was spilled on the surface and then the dielectric permittivity was measured to obtain a second map (Figure 7(b)). Comparison of the dielectric maps shown in Figures 6(a) and 6(b) confirms that the presence of contaminant cannot be inferred directly, even in this experiment under controlled laboratory conditions. Real dielectric permittivity deviations observed after comparing point by point on the twin samples at each testing location can be attributed either to small changes in soil sample properties such as changes in porosity and slight variations in soil initial water content or to the presence of paraffin oil. Hence, a decrease in κ' at any point in Figure 7(b) may be explained either by a small increase in sample porosity (which means an increase in air content with κ' = 1) or by the presence of paraffin oil (κ' = 2.01). This result indicates that when aiming to determine the presence of paraffin oil, this becomes very difficult when the soil samples in which measurements are performed are not the same and when initial conditions of κ' of the samples are not known in advance.

The contrast between the real dielectric permittivities of contaminated and uncontaminated soils becomes more important at higher volumetric fluid contents (when saturation approaches S = 1). Figure 8 shows the dielectric permittivity map for a heterogeneous sample of fine sand, in which the central

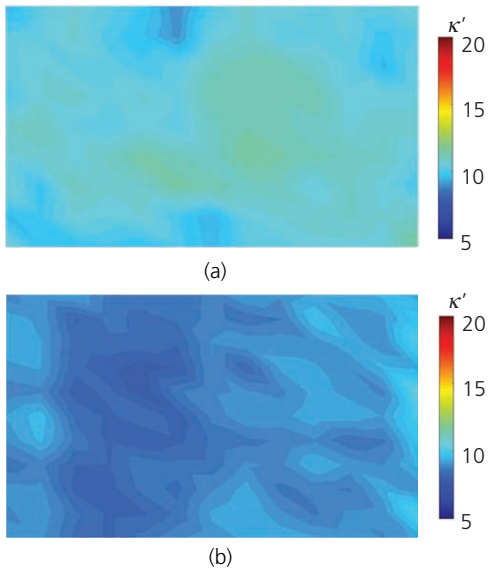

Figure 7. Real dielectric permittivity map (dimensionless) in a uniform fine sand sample with 5% water: (a) before the spill of oil; (b) after the spill of oil (second group of experiments)

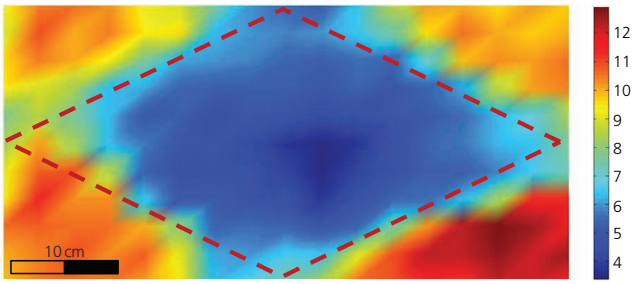

Figure 8. Real dielectric permittivity map in a uniform fine sand sample with a central rhombohedral region initially contaminated with paraffin oil (third group of experiments)

rhombohedral region was composed of sand with a moisture content of 25% paraffin oil by weight and the outer region of sand with a moisture content of 25% of water by weight (third group of experiments). The map of the dielectric permittivity measured clearly delineates the region intentionally filled with the sand–paraffin oil mixture. The real dielectric permittivities measured match well those shown in the calibration curves presented in Figure 4. The information shown in Figure 8 is the raw real dielectric permittivity data obtained with the CIDR device, which confirms that detection is possible under favourable conditions without the need of any sophisticated post-processing.

The results confirm that a significant amount of oil is required to be inside the pores for this to be detected by means of real dielectric permittivity measurements if the initial condition is not known in advance. However, if the initial real dielectric permittivity is known, the probability of success in detecting the presence of oil increases significantly due to the replacement of air ($\kappa' = 1$) or water ($\kappa' = 78.5$) by oil ($\kappa' = 2.01$). Thus, the challenge is not to measure the real dielectric permittivity of the soil but to monitor changes in κ'.

Figure 9 shows relative changes in the real dielectric permittivity of wet sand with an initial water moisture content of $w = 5\%$ (by weight) as a consequence of the paraffin oil spill indicated in Figure 3 for the fourth group of experiments performed. The initial real dielectric permittivity of the wet sand was $\kappa'_{sw} \approx 5$. The buried probe successfully detected increases in κ' over time while the paraffin oil was released. The sensor was able to detect the replacement of air by oil, which led to increases in the real dielectric permittivity as great as 20%, approximately. The presence of oil could be confirmed only because the initial stage was known, and an oil release was expected. Otherwise, the accuracy of measurements provides only differences in κ' like that shown in Figure 7, which cannot be attributed solely to the detection of oil contamination.

The results and procedure developed in this work show the convenience of using a dielectric sensor buried below oil tanks and pipelines, as an early detection system for monitoring unexpected and accidental leakages.

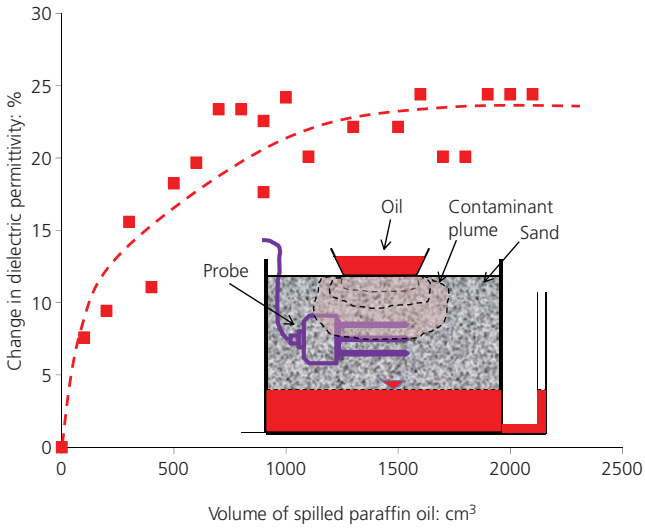

Figure 9. Changes in the real dielectric permittivity of sand under a continuous infiltration of paraffin oil (fourth group of experiments)

Conclusions

This study experimentally determined and modelled the real dielectric permittivities of sand–water and sand–paraffin oil mixtures. Physical models were tested to evaluate the ability of the HydraProbe soil sensor, using CIDR, to detect oil contamination in soils. The main conclusions can be summarised as follows.

- The real dielectric permittivity of soils is highly dependent on the volumetric contents and the real dielectric permittivity of the pore fluid. The CRIM formula is adequate to describe the fundamental behaviour of the mixtures for practical purposes. Francisca and Montoro's formula can be used to obtain a rapid preliminary quantification of the presence of oil inside the pores.
- The spatial variability of soil properties restricts the capacity of contaminant detection when the initial state is unknown. The influence of the spatial variability of soil properties, mainly porosity and liquid content, may induce changes similar to those expected due to the presence of oil inside the pores. This may hide the presence of oil and be a strong limitation for the detectability of soil contamination.
- It is possible to detect oil in water–wet sand by means of low-cost CIDR sensors if the initial real dielectric properties of the soil are known. Thus, the installation of dielectric sensors to monitor changes in κ' over time is the most important factor for success in early detection systems.
- The replacement of air by oil produces an increase in real dielectric property values up to 20%, and this can be measured with high accuracy by means of dielectric sensors.
- The accuracy of measurements increases with a higher volumetric content of liquids.

- The results obtained show that the dielectric sensor can be conceived as an early detection system to monitor unexpected and accidental leakages of oil. Permanently installed sensors are able to detect small changes in real permittivity and therefore can be used to analyse periodically possible changes that may be attributed to the presence of oil.

Acknowledgements

The authors would like to acknowledge the Consejo Nacional de Investigaciones Científicas y Técnicas, Fondo para la Investigación Científica y Tecnológica and Secretaría de Ciencia y Tecnología –Universidad Nacional de Córdoba, which collectively funded this project, and Agustina Krapp and Lisandro Capdevila for their help in performing some of the experiments presented here.

REFERENCES

Abousina RM, Manalo A, Shiau J *et al.* (2015) Effects of light crude oil contamination on the physical and mechanical properties of fine sand. *Soils and Sediment Contamination* **24(8)**: 933–845, https://doi.org/10.1080/15320383.2015.1058338.

Alimohammadi M, Tackley H, Holmes B *et al.* (2020) Characterising sediment physical property variability for bench-scale dewatering purposes. *Environmental Geotechnics*, https://doi.org/10.1680/jenge.19.00214.

ASTM (2017) D 2487: Standard practice for classification of soils for engineering purposes (Unified Soil Classification System). ASTM International, West Conshohocken, PA, USA.

Atekwana EA, Werkema DD and Atekwana EA (2006) Biogeophysics: the effects of microbial processes on geophysical properties of the shallow subsurface. In *Applied Hydrogeophysics* (Vereecken H, Binley A, Cassiani G, Revil A and Titov K (eds)). Springer, Dordrecht, the Netherlands, pp. 161–193.

Benson CH and Bosscher PJ (1999) Time-domain reflectometry (TDR) in geotechnics: a review. In *Nondestructive and Automated Testing for Soil and Rock Properties* (Marr WA and Fairhust CE (ed.)). ASTM International, West Conshohocken, PA, USA, ASTM STP1350, pp. 1–24.

Bore T, Mishra PN, Wagner N *et al.* (2021) Coupled hydraulic, mechanical and dielectric investigations on kaolin. *Engineering Geology* **294**: article 106352, https://doi.org/10.1016/j.enggeo.2021.106352.

Cao Q, Song X, Wu H *et al.* (2020) Mapping the response of volumetric soil water content to an intense rainfall event at the field scale using GPR. *Journal of Hydrology* **583**: article 124605, https://doi.org/10.1016/j.jhydrol.2020.124605.

Cardarelli E and Di Filippo G (2009) Electrical resistivity and induced polarization tomography in identifying the plume of chlorinated hydrocarbons in sedimentary formation: a case study in Rho (Milan–Italy). *Waste Management & Research* **27(6)**: 595–602, https://doi.org/10.1177/0734242X09102524.

Cassidy NJ (2007) Evaluating NAPL contamination using GPR signal attenuation analysis and dielectric properties measurements: practical implications for hydrological studies. *Journal of Contaminant Hydrology* **94(1–2)**: 49–75, https://doi.org/10.1016/j.jconhyd.2007.05.002.

Castelluccio M, Agrahari S, De Simone G *et al.* (2018) Using a multi-method approach based on soil radon deficit, resistivity, and induced polarization measurements to monitor non-aqueous phase liquid contamination in two study areas in Italy and India. *Environmental Science and Pollution Research* **25(13)**: 12515–12527, https://doi.org/10.1007/s11356-018-1429-0.

Cataldo A, Persico R, Leucci G *et al.* (2014) Time domain reflectometry, ground penetrating radar and electrical resistivity tomography: a comparative analysis of alternative approaches for leak detection in underground pipes. *NDT&E International* **62**: 14–28, https://doi.org/10.1016/j.ndteint.2013.10.007.

Cecconi A, Verginelli I and Baciocchi R (2022) Modeling of soil gas radon as an in situ partitioning tracer for quantifying LNAPL contamination. *Science of the Total Environment* **806**: article 150593, https://doi.org/10.1016/j.scitotenv.2021.150593.

Černý R (2009) Time-domain reflectometry method and its application for measuring moisture content in porous materials: a review. *Measurement* **42(3)**: 329–336, https://doi.org/10.1016/j.measurement.2008.08.011.

Colombano S, Davarzani H, van Hullebusch ED *et al.* (2020) Thermal and chemical enhanced recovery of heavy chlorinated organic compounds in saturated porous media: 1D cell drainage-imbibition experiments. *Science of the Total Environment* **706**: article 135758, https://doi.org/10.1016/j.scitotenv.2019.135758.

Colombano S, Davarzani H, van Hullebusch ED *et al.* (2021) Permittivity and electrical resistivity measurements and estimations during the recovery of DNAPL in saturated porous media: 2D tank experiments. *Journal of Applied Geophysics* **191**: article 104359, https://doi.org/10.1016/j.jappgeo.2021.104359.

Comegna A, Coppola A, Dragonetti G *et al.* (2013) Dielectric response of a variable saturated soil contaminated by non-aqueous phase liquids (NAPLs). *Procedia Environmental Sciences* **19**: 701–710, https://doi.org/10.1016/j.proenv.2013.06.079.

Comegna A, Coppola A, Dragonetti G and Sommella A (2016) Estimating nonaqueous-phase liquid content in variably saturated soils using time domain reflectometry. *Vadose Zone Journal* **15(5)**: 1–11, https://doi.org/10.2136/vzj2015.11.0145.

Comegna A, Coppola A, Dragonetti G *et al.* (2019) A soil non-aqueous phase liquid (NAPL) flushing laboratory experiment based on measuring the dielectric properties of soil–organic mixtures via time domain reflectometry (TDR). *Hydrology and Earth System Sciences* **23(9)**: 3593–3602, https://doi.org/10.5194/hess-23-3593-2019.

Coulon F, Whelan MJ, Paton GI *et al.* (2010) Multimedia fate of petroleum hydrocarbons in the soil: oil matrix of constructed biopiles. *Chemosphere* **81(11)**: 1454–1462, https://doi.org/10.1016/j.chemosphere.2010.08.057.

Davidson KB, Lake CB, Sweet B *et al.* (2021) Examining the ultraviolet optical screening tool as a viable means for delineating a contaminated organic sediment. *Science of the Total Environment* **799**: article 149408, https://doi.org/10.1016/j.scitotenv.2021.149408.

Davis E, Walker TR, Adams M *et al.* (2018) Characterization of polycyclic aromatic hydrocarbons (PAHs) in small craft harbour (SCH) sediments in Nova Scotia, Canada. *Marine Pollution Bulletin* **137**: 285–294, https://doi.org/10.1016/j.marpolbul.2018.10.043.

Dawrea A, Zytner RG and Donald J (2021) Enhanced GPR data interpretation to estimate in situ water saturation in a landfill. *Waste Management* **120**: 175–182, https://doi.org/10.1016/j.wasman.2020.11.033.

Deceuster J and Kaufmann O (2012) Improving the delineation of hydrocarbon-impacted soils and water through induced polarization (IP) tomographies: a field study at an industrial waste land. *Journal of Contaminant Hydrology* **136–137**: 25–42, https://doi.org/10.1016/j.jconhyd.2012.05.003.

Deng YP, Shi XQ, Xu HG *et al.* (2017) Quantitative assessment of electrical resistivity tomography for monitoring DNAPLs migration – comparison with high-resolution light transmission visualization in laboratory sandbox. *Journal of Hydrology* **544**: 254–266, https://doi.org/10.1016/j.jhydrol.2016.11.036.

Dirksen C and Dasberg S (1993) Improved calibration of time domain reflectometry soil water content measurements. *Soil Science Society of America Journal* **57(3)**: 660–667, https://doi.org/10.2136/sssaj1993.03615995005700030005x.

Endres A and Knight R (1992) A theoretical treatment of the effect of microscopic fluid distribution on the dielectric properties of partially

saturated rocks. *Geophysical Prospecting* **40(3)**: 307–324, https://doi.org/10.1111/j.1365-2478.1992.tb00377.x.

Estrabagh AR, Beytolahpour I, Moradi M *et al.* (2014) Consolidation behavior of two fine-grained soils contaminated by glycerol and ethanol. *Engineering Geology* **178**: 102–108, https://doi.org/10.1016/j.enggeo.2014.05.017.

Farthing MW, Seyedabbasi MA, Imhoff PT and Miller CT (2012) Influence of porous media heterogeneity on nonaqueous phase liquid dissolution fingering and upscaled mass transfer. *Water Resources Research* **48(8)**: article W08507, https://doi.org/10.1029/2011WR011389.

Fernandez F and Quigley RM (1985) Hydraulic conductivity of natural clays permeated with simple liquid hydrocarbons. *Canadian Geotechnical Journal* **22(2)**: 205–214, https://doi.org/10.1139/t85-028.

Flores Orozco A, Kemma A, Oberdörster C *et al.* (2012) Delineation of subsurface hydrocarbon contamination at a former hydrogenation plant using spectral induced polarization imaging. *Journal of Contaminant Hydrology* **136–137**: 131–144, https://doi.org/10.1016/j.jconhyd.2012.06.001.

Francisca FM (2001) *Evaluation of Contaminated Soils with Organic Fluids by Means of Electromagnetic Waves*. PhD thesis, Universidad Nacional de Córdoba, Cordoba, Argentina (in Spanish).

Francisca FM and Montoro MA (2012) Measuring the dielectric properties of soil–organic mixtures using coaxial impedance dielectric reflectometry. *Journal of Applied Geophysics* **80**: 101–109, https://doi.org/10.1016/j.jappgeo.2012.01.011.

Francisca FM and Montoro MA (2015) Influence of particle size distribution, and wettability on the displacement of LNAPL in saturated sandy soils. *Journal of Environmental Engineering* **141(6)**: article 04014091-4, https://doi.org/10.1061/(ASCE)EE.1943-7870.0000915.

Francisca FM and Rinaldi VA (2001) The potential application of the GPR to detect organic contaminants in sand. *Proceedings of the Fifteenth International Conference on Soil Mechanics and Geotechnical Engineering, Istanbul, Turkey*, pp. 405–408.

Francisca FM and Rinaldi VA (2003) Complex dielectric permittivity of soil–organic mixtures (20 MHz–1.3 GHz). *Journal of Environmental Engineering* **129(4)**: 347–357, https://doi.org/10.1061/(ASCE)0733-9372(2003)129:4(347).

Francisca FM, Montoro MA, Krapp A *et al.* (2012) Detection of LNAPLs by means of amplitude domain reflectometry. In *Geotechnical and Geophysical Site Characterization 4* (Coutinho P and Mayne PW (eds)). CRC Press, London, UK, pp. 1805–1810.

Glaser DR, Werkema DD, Versteeg RJ *et al.* (2012) Temporal GPR imaging of an ethanol release within a laboratory-scaled sand tank. *Journal of Applied Geophysics* **86**: 133–145, https://doi.org/10.1016/j.jappgeo.2012.07.016.

Glaser DR, Henderson RD, Werkema DD *et al.* (2022) Estimating biofuel contaminant concentration from 4D ERT with mixing models. *Journal of Contaminant Hydrology* **248**: article 104027, https://doi.org/10.1016/j.jconhyd.2022.104027.

Gnanapragasam N, Lewis BG and Finno R (1995) Microstructural changes in sand–bentonite soils when exposed to aniline. *Journal of Geotechnical Engineering* **121(2)**: 119–125, https://doi.org/10.1061/(ASCE)0733-9410(1995)121:2(119).

Govindarajan D, Deshpande AP and Raghunathan R (2018) Enhanced mobility of non aqueous phase liquid (NAPL) during drying of wet sand. *Journal of Contaminant Hydrology* **209**: 1–13, https://doi.org/10.1016/j.jconhyd.2017.12.005.

Gupta PK, Gharedaghloo B, Lynch M *et al.* (2020) Dynamics of microbial populations and diversity in NAPL contaminated peat soil under varying water table conditions. *Environmental Research* **191**: article 110167, https://doi.org/10.1016/j.envres.2020.110167.

Halihan T, Sefa V, Sale T *et al.* (2017) Mechanism for detecting NAPL using electrical resistivity imaging. *Journal of Contaminant Hydrology* **205**: 57–69, https://doi.org/10.1016/j.jconhyd.2017.08.007.

He H, Turner HC, Aogu K *et al.* (2021) Time and frequency domain reflectometry for the measurement of tree stem water content: a review, evaluation, and future perspectives. *Agricultural and Forest Meteorology* **306**: article 108442, https://doi.org/10.1016/j.agrformet.2021.108442.

Johansson S, Fiandaca G and Dahlin T (2015) Influence of non-aqueous phase liquid configuration on induced polarization parameters: conceptual models applied to a time-domain field case study. *Journal of Applied Geophysics* **123**: 295–309, https://doi.org/10.1016/j.jappgeo.2015.08.010.

Kaatze U (1993) Dielectric spectroscopy of aqueous solutions. Hydration phenomena and hydrogen-bonded networks. *Journal of Molecular Liquids* **56**: 95–115, https://doi.org/10.1016/0167-7322(93)80020-V.

Kafarski M, Majcher J, Wilczek A *et al.* (2019) Penetration depth of a soil moisture profile probe working in time-domain transmission mode. *Sensors* **19(24)**: article 5485, https://doi.org/10.3390/s19245485.

Kermani M and Ebadi T (2012) The effect of oil contamination on the geotechnical properties of fine-grained soils. *Soil and Sediment Contamination* **21(5)**: 655–671, https://doi.org/10.1080/15320383.2012.672486.

Kessouri P, Johnson T, Day-Lewis FD *et al.* (2022) Post-remediation geophysical assessment: investigating long-term electrical geophysical signatures resulting from bioremediation at a chlorinated solvent contaminated site. *Journal of Environmental Management* **302**: article 113944, https://doi.org/10.1016/j.jenvman.2021.113944.

Khamehchiyan M, Charkhabi AH and Tajik M (2007) Effects of crude oil contamination on geotechnical properties of clayey and sandy soils. *Engineering Geology* **89(3–4)**: 220–229, https://doi.org/10.1016/j.enggeo.2006.10.009.

Knight RM (2001) Ground penetrating radar for environmental applications. *Annual Review of Earth and Planetary Science* **29**: 229–255, https://doi.org/10.1146/annurev.earth.29.1.229.

Koohbor B, Deparis J, Leroy P *et al.* (2022) DNAPL flow and complex electrical resistivity evolution in saturated porous media: a coupled numerical simulation. *Journal of Contaminant Hydrology* **248**: article 104003, https://doi.org/10.1016/j.jconhyd.2022.104003.

Lau PKW, Cheung BWY, Lai WWL and Sham JFC (2021) Characterizing pipe leakage with a combination of GPR wave velocity algorithms. *Tunnelling and Underground Space Technology* **109**: article 103740, https://doi.org/10.1016/j.tust.2020.103740.

Lee SG, Kim BJ, Choi JW *et al.* (2019) Detection of oil release in unsaturated soil and estimation of oil infiltration rate using hydraulic control system and water content sensor. *Water, Air, & Soil Pollution* **230(4)**: 1–13, https://doi.org/10.1007/s11270-019-4147-4.

Le Meur M, Cohen GJ, Laurent M *et al.* (2021) Effect of NAPL mixture and alteration on 222Rn partitioning coefficients: implications for NAPL subsurface contamination quantification. *Science of the Total Environment* **791**: article 148210, https://doi.org/10.1016/j.scitotenv.2021.148210.

Lim MW, Von Lau E and Poh PE (2016) A comprehensive guide of remediation technologies for oil contaminated soil – present works and future directions. *Marine Pollution Bulletin* **109(1)**: 14–45, https://doi.org/10.1016/j.marpolbul.2016.04.023.

Liu L, Ju Y and Chen M (2013) Optimizing the frequency range of microwaves for high-resolution evaluation of wall thinning locations in a long-distance metal pipe. *NDT&E International* **57**: 52–57, https://doi.org/10.1016/j.ndteint.2013.03.007.

Macdonald JR and Johnson WB (1987) Fundamentals of impedance spectroscopy. In *Impedance spectroscopy Emphasizing Solid Materials and Systems* (Macdonald JR (ed.)). Wiley. New York, NY, USA, pp. 1–26.

Mohamed AO and Paleologos EK (2018) *Fundamentals of Geoenvironmental Engineering: Understanding Soil, Water, and Pollutant Interaction and Transport*. Elsevier, Oxford, UK.

Montoro MA and Francisca FM (2008) Detection of soil contamination by means of non-destructive techniques. *Proceedings of the XX Argentinean Conference on Soil Mechanics and Geotechnical Engineering, La Plata, Argentina*, pp. 233–241 (in Spanish).

Montoro MA and Francisca FM (2010) Soil permeability controlled by particle–fluid interaction. *Geotechnical and Geological Engineering* **28(6)**: 851–864, https://doi.org/10.1007/s10706-010-9348-y.

Mu QY, Zhan LT, Lin CP *et al.* (2020) Non-invasive time domain reflectometry probe for transient measurement of water retention curves in structured soils. *Engineering Geology* **264**: article 105335, https://doi.org/10.1016/j.enggeo.2019.105335.

Nemarich C (2001) Timedomain reflectometry liquid level sensors. *IEEE Instrumentation & Measurement Magazine* **4(4)**: 40–44, https://doi.org/10.1109/5289.975464.

Newell CJ, Acree SD, Ross RR *et al.* (1995) *Light Non-aqueous Phase Liquids*. US Environmental Protection Agency, Washington, DC, USA, EPA Ground Water Issue, EPA/540/S-95/500.

Parkhomenko EI (1967) Electrical Properties of Rocks. Springer, New York, NY, USA.

Persson M and Berndtsson R (2002) Measuring nonaqueous phase liquid saturation in soil using time domain reflectometry. *Water Resources Research* **38(5)**: 22.1–22.8, https://doi.org/10.1029/2001WR000523.

Power C, Gerhard JI, Karaoulis M *et al.* (2014) Evaluating four-dimensional time-lapse electrical resistivity tomography for monitoring DNAPL source zone remediation. *Journal of Contaminant Hydrology* **162**: 27–46, https://doi.org/10.1016/j.jconhyd.2014.04.004.

Power C, Gerhard JI, Tsourlos P *et al.* (2015) Improved time-lapse electrical resistivity tomography monitoring of dense non-aqueous phase liquids with surface-to-horizontal borehole arrays. *Journal of Applied Geophysics* **112**: 1–13, https://doi.org/10.1016/j.jappgeo.2014.10.022.

Puri VK (2000) Geotechnical aspects of oil – contaminated sands. *Soil and Sediment Contamination* **9(4)**: 359–374, https://doi.org/10.1080/10588330091134301.

Ramezanzadeh M, Aminnaji M, Rezanezhad F *et al.* (2022) Dissolution and remobilization of NAPL in surfactant-enhanced aquifer remediation from microscopic scale simulations. *Chemosphere* **289**: article 133177, https://doi.org/10.1016/j.chemosphere.2021.133177.

Redman JD, Kueper BH and Annan AP (1991) Dielectric stratigraphy of a DNAPL spill and implications for detection with ground penetrating radar. *Ground Water Management* **5**: 1017–1030.

Revil A, Karaoulis M, Johnson T *et al.* (2012) Review: Some low-frequency electrical methods for subsurface characterization and monitoring in hydrogeology. *Hydrogeology Journal* **20**: 617–658, https://doi.org/10.1007/s10040-011-0819-x.

Rinaldi VA and Francisca FM (1999) Impedance analysis of soil dielectric dispersion (1 MHz to 1 GHz). *Journal of Geotechnical Engineering* **125(2)**: 111–121, https://doi.org/10.1061/(ASCE)1090-0241(1999)125:2(111).

Rinaldi VA and Francisca FM (2006) Removal of immiscible contaminants from sandy soils monitored by means of dielectric measurements. *Journal of Environmental Engineering* **132(8)**: 931–939, https://doi.org/10.1061/(ASCE)0733-9372(2006)132:8(931).

Santamarina JC and Fam M (1997) Dielectric permittivity of soils mixed with organic and inorganic fluids (0,02 GHz to 1,3 GHz). *Journal of Environmental & Engineering Geophysics* **2(1)**: 37–51, https://doi.org/10.4133/JEEG2.1.37.

Seyfried MS and Murdock MD (2004) Measurement of soil water content with a 50-MHz soil dielectric sensor. *Soil Science Society of American Journal* **68(2)**: 394–403, https://doi.org/10.2136/sssaj2004.3940.

Seyfried MS, Grant LE, Du E *et al.* (2005) Dielectric loss and calibration of the hydra probe soil water sensor. *Vadose Zone Journal* **4(4)**: 1070–1079, https://doi.org/10.2136/vzj2004.0148.

Sharma HD and Reddy KR (2004) *Geoenvironmental Engineering*. Wiley, Hoboken, NJ, USA.

Sharma P, Kostarelos K, Lenschow S *et al.* (2020) Surfactant flooding makes a comeback: results of a full-scale, field implementation to recover mobilized NAPL. *Journal of Contaminant Hydrology* **230**: article 103602, https://doi.org/10.1016/j.jconhyd.2020.103602.

Singha K, Day-Lewis FD, Johnson T *et al.* (2015) Advances in interpretation of subsurface processes with time-lapse electrical imaging. *Hydrological Processes* **29(6)**: 1549–1576, https://doi.org/10.1002/hyp.10280.

Suchorab Z, Majerek D, Kočí V *et al.* (2020) Time domain reflectometry flat sensor for non-invasive monitoring of moisture changes in building materials. *Measurement* **165**: article 108091, https://doi.org/10.1016/j.measurement.2020.108091.

Thevanayagam S (1995) Frequency-domain analysis of electrical dispersion of soils. *Journal of Geotechnical Engineering* **121(8)**: 618–628, https://doi.org/10.1061/(ASCE)0733-9410(1995)121:8(618).

Topp GC, Davis JL and Annan AP (1980) Electromagnetic determination of soil water content: measurement in coaxial transmission lines. *Water Resources Research* **16(3)**: 574–582, https://doi.org/10.1029/WR016i003p00574.

Tsai Y, Chou Y, Eu Y *et al.* (2020) Noninvasive survey technology for LNAPL-contaminated site investigation. *Journal of Hydrology* **587**: article 125002, https://doi.org/10.1016/j.jhydrol.2020.125002.

Xie F, Lai EEL and Dérobert X (2020) GPR-based depth measurement of buried objects based on constrained least-square (CLS) fitting method of reflections. *Measurement* **168**: article 108330, https://doi.org/10.1016/j.measurement.2020.108330.

Yoon YY, Koh DC, Lee KY *et al.* (2013) Using ^{222}Rn as a naturally occurring tracer to estimate NAPL contamination in an aquifer. *Applied Radiation and Isotopes* **81**: 233–237, https://doi.org/10.1016/j.apradiso.2013.03.061.

How can you contribute?

To discuss this paper, please submit up to 500 words to the editor at journals@ice.org.uk. Your contribution will be forwarded to the author(s) for a reply and, if considered appropriate by the editorial board, it will be published as a discussion in a future issue of the journal.